Research Square

Preprints are preliminary reports that have not undergone peer review.
They should not be considered conclusive, used to inform clinical practice,
or referenced by the media as validated information.

Shallow marine warmth persisted across the Cretaceous–Paleogene boundary in the United States Gulf Coastal Plain

Adriana J. Brown

abrownn@umich.edu

University of Michigan

Samantha Davies

University of Michigan

Sierra V. Petersen

University of Michigan

James D. Witts

Natural History Museum

Corinne Myers

University of New Mexico

Carlie Piestch

San Jose State University

Jonathan Hoffman-Vinje

University of Michigan

Jone Naujokaityte

University of New Mexico

Matthew Garb

Brooklyn College

Neil Landman

American Museum of Natural History

Paul Bown

University College London

Christopher M. Lowery

The University of Texas at Austin

Lorna Kearns

The University of Texas at Austin

Article

Keywords:

Posted Date: November 20th, 2026

DOI: https://doi.org/10.21203/rs.3.rs-11613019/v1

License: This work is licensed under a Creative Commons Attribution 4.0 International License.
Read Full License

Additional Declarations: No competing interests reported.

Shallow marine warmth persisted across the Cretaceous–Paleogene boundary in the United States Gulf Coastal Plain

Adriana J. Brown (United States), Samantha Davies (United States), Sierra Petersen (United States), James D. Witts (United Kingdom), Corinne Myers (United States), Carlie Pietsch (United States), Jonathan Hoffman-Vinje (United States), Jone Naujokaityte (United States), Matthew Garb (United States), Neil Landman (United States), Paul Bown (United Kingdom), Christopher M. Lowery (United States) & Lorna Kearns (United States)

Corresponding author: Adriana J. Brown (abrownn@umich.edu)

ABSTRACT

The Gulf Coastal Plain (GCP) of North America contains an exceptionally complete shallow marine record of the Cretaceous-Paleogene (K-Pg) mass extinction. Fine-scale biotic and environmental changes across the K-Pg have been well-documented; however, the long-term climate of the GCP before and after the impact—and its influence on biotic recovery and repopulation—remains ambiguous. To constrain the backdrop, timing, and magnitude of climatic changes across the K-Pg, we applied carbonate clumped isotope paleothermometry (Δ_{47}) to 111 bivalve samples collected from eight shallow marine sites in the GCP. This study is, to our knowledge, the first long-term and multi-environment record across a major extinction boundary based on the Δ_{47} of marine macro-invertebrates. Broadly, we find that average seawater temperatures remained warm (~25 ˚C) at long time scales (10–100 kyr) before and after the K-Pg. We provide preliminary evidence from high-resolution temperature records at several sites that the Late Maastrichtian Warming Event (LMWE) was present in the GCP and may have been more intense than previously suggested. These results are supported by reconstructed oxygen

isotope compositions of seawater ($\delta^{18}O_w$), which were heavier than that traditionally assumed for the Cretaceous (> -1‰) and covaried with temperature through time. Together, our temperature and $\delta^{18}O_w$ records imply that the physical climate recovered relatively quickly (within ~100 kyr) after the impact, and that biotic and ecological variables, not long-term temperature change, may have been the key drivers of long-term ecosystem turnover, restructuring, and rebound.

INTRODUCTION

The Cretaceous-Paleogene (K-Pg) boundary is marked by the catastrophic impact of an asteroid on the Yucatán platform 66 million years ago.[1,2,3,4,5,6] Immediately after the impact, Earth experienced the release and reentry of gigatons of ejecta, widespread slope failure and soil liquefaction, massive wildfires, a magnitude-11 earthquake, and a megatsunami.[7,8,9,10,11,12] The release of sulfate aerosols, soot, and dust drove an intense "impact winter," wherein the planet underwent years-to-decades of widespread darkening, global cooling, and ocean acidification.[8,13,14,15,16] The combined physical effects of the impact led to the Cretaceous-Paleogene (K-Pg) mass extinction, during which over 75% of all species in the fossil record were lost.[1,4,17,18] After the impact, marine ecosystems required extended periods of time to recover, with elevated export production lasting 160 kyr in the Gulf Coastal Plain[19] (300 kyr in the Gulf of Mexico[20]), and the global biological pump at a weakened state for 1.8 Ma.[21] As the most recent mass extinction, the K-Pg event serves as a uniquely complete and high-resolution archive to understand how life and the environment changed in the aftermath of a rapid global disaster.[4]

The Gulf Coastal Plain of North America (GCP) is a classic site of K-Pg research due to its long-term geologic stability,[22,23] proximity to the site of the Chicxulub impact (~1500 km),[4,24] and relatively complete and exceptionally fossiliferous successions spanning multiple marine

45 environments.[25,26] A large body of previous work has sought to unravel complex event
46 stratigraphy,[4,27,28] investigate regional and site-specific biostratigraphy, [25,29,30,31,32] identify and
47 correlate K-Pg boundary deposits,[24,28,33,34] and reconstruct paleoenvironmental and ecosystem
48 dynamics.[19,35,36,37,38] However, traditional paleotemperatures proxies have been unable to resolve
49 the long-term climate surrounding the K-Pg in the GCP.[15,35,43] The carbonate clumped isotope
50 (Δ_{47}) paleothermometer, which depends solely on the thermodynamically controlled abundance
51 of multiple heavy isotope substitutions within a carbonate ion, can provide independent estimates
52 of paleotemperatures and seawater oxygen isotope compositions ($\delta^{18}O_w$)—allowing for more
53 accurate quantifications of paleoclimate conditions.[39,40,41,42]

54 This study applies Δ_{47} paleothermometry to 111 bivalves from eight sites in the GCP to
55 create the first regionally extensive, multi-environment, long-term temperature and $\delta^{18}O_w$ record
56 across any boundary of a "Big 5" mass extinction (Figs. 1 and 2). Using recently developed age
57 models and field-based high-resolution stratigraphic sampling (outlined in detail in the
58 Supplemental Material) we illustrate how the climate of the GCP evolved between the latest
59 Cretaceous and earliest Paleogene, at time scales of 10s to 100s of kyr and across a variety of
60 shallow marine environments (Fig. 3; Table 1). We find that temperatures returned to
61 Cretaceous-level warmth by ~100 kyr post-impact and that $\delta^{18}O_w$ was almost always isotopically
62 heavier than -1‰, the traditional assumption for a globally-averaged ice-free ocean.[43]
63 Additionally, this study offers preliminary characterization of the Late Maastrichtian Warming
64 Event (LMWE) in the GCP and compares this to previous estimates of warming from traditional
65 stable oxygen isotopes (Fig. 4). Overall, our findings reveal that the physical climate returned to
66 equilibrium geologically quickly after the K-Pg impact event, even in sites relatively close to the

Chicxulub crater, implying that other environmental and ecological factors may have significantly governed biotic responses on longer timescales after the catastrophe.

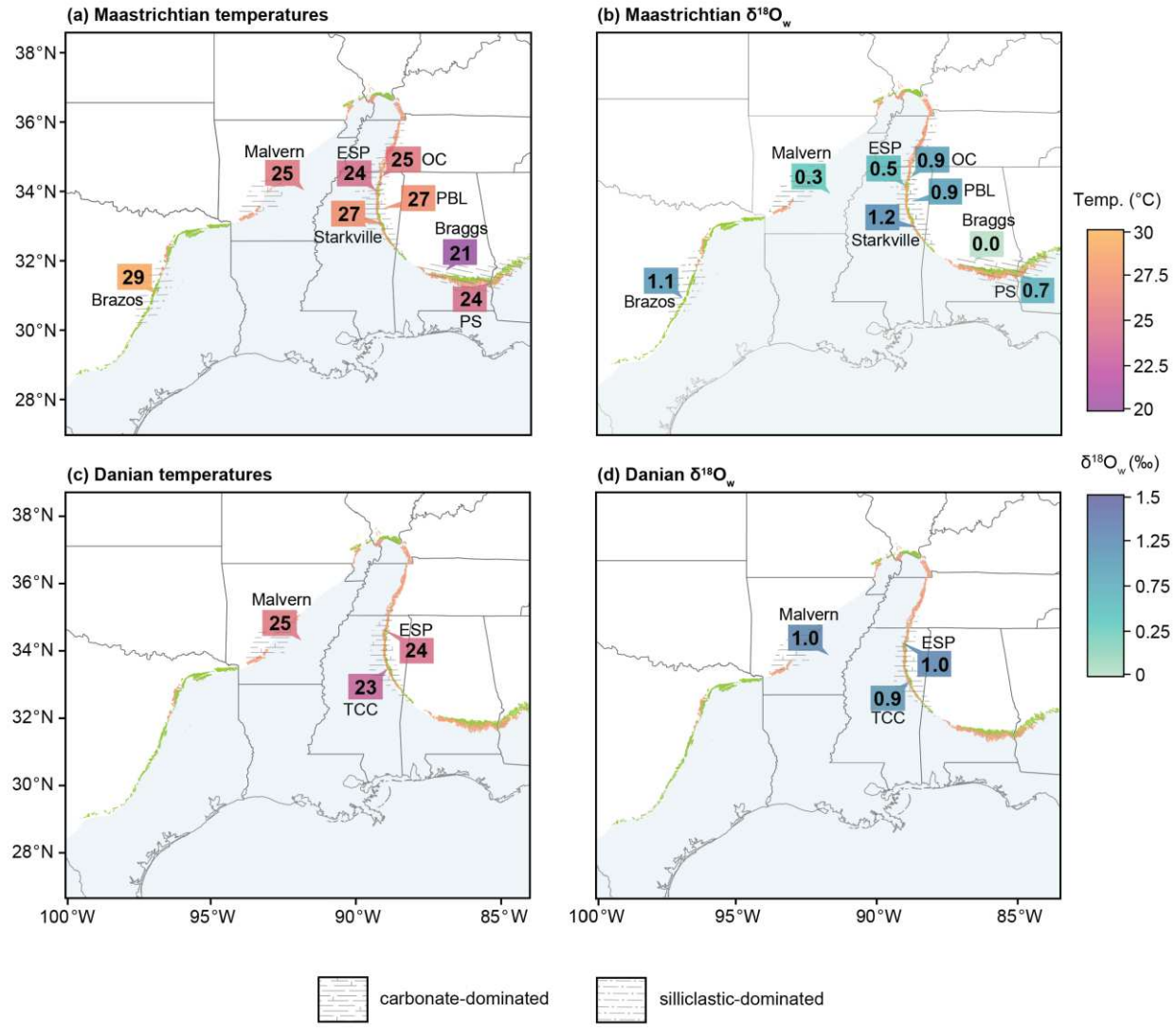


Figure 1. Map of the Gulf Coastal Plain with average temperature and $\delta^{18}O_w$ values at each site. Maastrichtian and Danian outcrops along the paleo-coastline are colored in green and orange, respectively.[44,45] Patterning around each site represents a siliciclastic- or carbonate-dominated locality. Each site is labelled with and shaded according to the average temperature and $\delta^{18}O_w$ in the Maastrichtian or Danian (panels a–d). Abbreviations are as follows: ESP–Ellis

Table 1. Results summarized by site.

Site	Stage	Formation	Environment	Mean Temperature[1] (°C) [95% CI]	Mean $\delta^{18}O_w$[1] (‰) [95% CI]	n[2]
Braggs	Maastrichtian	Prairie Bluff Chalk	Inner-middle shelf	21.2 ± 3	0.02 ± 0.3	3
Brazos	Maastrichtian	Corsicana Formation	Middle-outer shelf	29.0 ± 5	1.09 ± 0.7	7
Ellis Sand Pit	Danian	Clayton Formation	Inner shelf	23.7 ± 2	1.02 ± 0.6	5
Ellis Sand Pit	Maastrichtian	Owl Creek Formation	Inner-middle shelf	23.9 ± 1	0.49 ± 0.3	13
Malvern	Danian	Clayton Formation	Inner-middle shelf	25.0 ± 2	1.04 ± 0.4	5
Malvern	Maastrichtian	Arkadelphia Marl	Inner-middle shelf	24.7 ± 3	0.35 ± 0.5	14
Owl Creek Type Section	Maastrichtian	Owl Creek Formation	Inner-middle shelf	25.1 ± 2	0.91 ± 0.5	18
PB Landfill	Maastrichtian	Prairie Bluff Chalk	Middle-outer shelf	27.1 ± 5	0.86 ± 2.0	3
Starkville	Maastrichtian	Prairie Bluff Chalk	Middle-outer shelf	26.9 ± 2	1.27 ± 0.3	11
Trim Cane Creek	Danian	Clayton Formation	Inner-middle shelf	23.4 ± 2	0.86 ± 0.7	12
Providence Sand	Maastrichtian	Providence Sand Formation	Outer shelf?[3]	23.4 ± 2	0.58 ± 0.5	20

[1]Mean values are reported with the 95% confidence interval (CI), as described in the Methods section.

[2]Includes only well-preserved samples that passed preservation screening.

[3]As museum specimens did not possess stratigraphic information, we assumed an outer-shelf depositional environment based on analysis of the Providence Sand Formation in King et al. (1991).[46]

Sand Pit; OC–Owl Creek Type Section; PBL–Prairie Bluff Landfill; PS–Providence Sand; TCC–Trim Cane Creek. For detailed site descriptions, refer to the supplemental text.

RESULTS

Temperature of the GCP

In this and all following sections, averages are reported as the 95% confidence interval of the population mean. We find no significant difference between average Maastrichtian and Danian temperatures in the GCP (24–26 ˚C [n = 89] versus 22–25 ˚C [n = 22], respectively) and that regional averages were comparable to modern GCP average annual sea surface temperatures (24–26 ˚C; NOAA CoastWatch 2026 https://www.nnvl.noaa.gov/view/globaldata.html#SURF). The warmest Maastrichtian localities were in middle-to-outer shelf deposits in central Mississippi (Starkville) and east Texas (Brazos) and averaged 25–29 ˚C (n = 11) and 24–34 ˚C (n = 7), respectively (Fig. 1; Table 1). The Malvern site in Central Arkansas, interpreted as inner-to-middle shelf paleoenvironment, recorded the warmest Danian site average (23–27 ˚C; n = 6). Temperatures were largely statistically indistinguishable between environments (p = 0.07–0.99), a summary of which can be found in the supplemental text (Fig. S11 and Table S1 and S2). The middle-to-inner shelf, which was the most highly sampled paleoenvironment and the only one represented by both Maastrichtian and Danian samples, remained at 24 ˚C across the boundary.

Temperatures from previous Δ_{47} studies in the nearby Western Interior Seaway (WIS) and GCP generally agree with data in this study. Previous Δ_{47} work in the southernmost WIS (Brown et al., *in press*) found average temperatures of 22–32 ˚C in the Maastrichtian (n = 41), a range which includes the Maastrichtian GCP average reported here. Brazos site samples were previously published in Brown et al. (*in press*); however, excluding those samples in the above comparison yields the same result. Meyer et al. (2018; updated in Jones et al., 2022), calculated an average temperature of 18–24 ˚C from samples collected from the Maastrichtian Prairie Bluff Chalk at Moscow Landing and Marengo County, Alabama.[47,48] Our samples from nearby sites

within the Prairie Bluff Chalk (Braggs and Starkville) together averaged 24–26 ˚C (n = 23), similar to, although slightly warmer than, Meyer et al. (2018). However, Meyer et al. (2018) may underestimate temperatures due to predating current interlaboratory Δ_{47} standards, especially those defining the absolute reference frame.[49,50,51,52] See supplementary text in Brown et al. (*in press*) for further discussion.

Previous alkenone-based paleotemperature estimates in the GCP are often warmer than those reported here.[16,53,54] O'Brien et al. (2017) compiled and reanalyzed TEX_{86} data from Linnert et al. (2014) and Vellekoop et al. (2014), reporting average temperatures of 30–35 ˚C from the Shuqualak–Evans borehole in Mississippi and 31–33 ˚C for the Brazos site.[16,53,54] Our Maastrichtian sites in Mississippi (PB Landfill, Owl Creek Type Section, Ellis Sand Pit, and Starkville) averaged 24–26 ˚C (n = 45), with Brazos mean temperatures between 24–34 ˚C (n = 7; Fig. 1). Discrepancies within TEX_{86} paleotemperature results and in comparison to Δ_{47} could arise from the choice of calibration methods, samples capturing different environments (i.e., seafloor vs. sea surface), or as a reflection of warm-biases observed in previous Cretaceous TEX_{86} studies.[55,56,57]

While only a limited number of studies have applied $\delta^{18}O$ paleothermometry to samples from the GCP across the K-Pg, we find that existing estimates are several degrees (~5–10 ˚C) cooler than our Δ_{47}-derived temperatures at the same or nearby sites.[35,58] Zachos et al. (1989) and Sessa et al. (2015) found that seafloor temperatures remained at ~19 ˚C at the Braggs and Owl Creek Type Section localities based on the $\delta^{18}O$ of benthic micro- and macrofossils. We calculate mean temperatures of 18–26 ˚C (n = 3) and 24–26 ˚C (n = 18) at the Braggs site and Owl Creek Type Section, respectively. Importantly, these studies used standard "ice-free" $\delta^{18}O_w$ assumptions of -1‰[59] or -1.2‰.[35] If the assumed $\delta^{18}O_w$ was heavier than -1‰ (as our data

strongly supports), temperatures calculated from this published $\delta^{18}O_c$ data would likely increase by several degrees and align with our Δ_{47}-based temperature estimates (Fig. 4).[59,60,61]

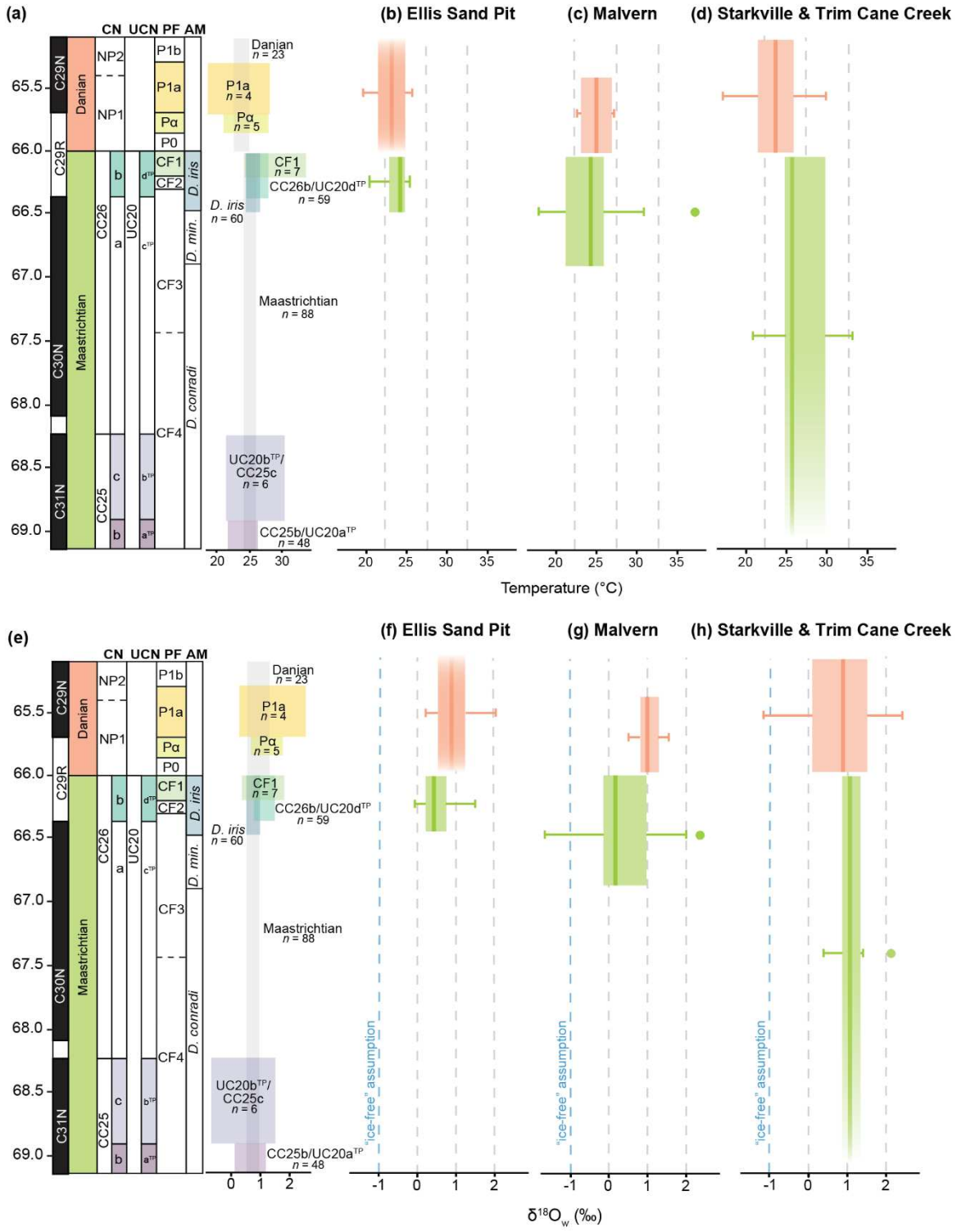


Figure 2. Temperature and $\delta^{18}O_w$ trends summarized by biostratigraphic zone and site. Panels a) and e) summarize biostratigraphy and age models of the GCP (abbreviations as follows: CN–calcareous nannofossils, UCN–Upper Cretaceous Nannofossils, PF–planktic foraminifera, AM–ammonoids). The 95% confidence interval of the biozone mean temperature or $\delta^{18}O_w$ are shaded in color, while grey shading represents stage means. Panels b–d) and f–h) summarize temperature and $\delta^{18}O_w$ in the Maastrichtian versus the Danian, with the height of the boxplot corresponding to biozones covered at each site.

$\delta^{18}O_w$ of the GCP

All isotopic compositions reported here are given relative to Vienna Standard Mean Ocean Water (VSMOW). Average $\delta^{18}O_w$ across the GCP was relatively enriched in ^{18}O and statistically indistinguishable ($p = 0.36$) between the Maastrichtian and Danian (0.5–0.9‰ [$n = 89$] versus 0.6–1.3‰ [$n = 22$]) and environments ($p = 0.15$; Table S1). These values are within range of those calculated for the southernmost WIS (-0.2–1.4‰, $n = 41$; Brown et al., in review) and from previous work in Alabama (-0.1–1.3‰; Prairie Bluff Chalk).[47,48] We find all but three samples in this study had $\delta^{18}O_w$ values greater than or equal to -1.0‰ (Fig. 2) as calculated using calibrations in Kim et al. (2007) and Kim and O'Neil (1997; see Methods).[43] We compared these two calibrations with four others: Bemis et al. (1998), Grossman (2012), and Grossman and Ku (1986; updated in Dettman et al., 1999), and Daëron et al. (2019; (Fig. S14; Table S4).[60,62,63,64,65] All calibrations yielded $\delta^{18}O_w$ values significantly greater than -1.0‰ ($p < .001$) except for Daëron et al. (2019), which gave an average $\delta^{18}O_w$ of -0.9‰, potentially from its use of karstic and mammillary calcite rather than biogenic or synthetic calcium carbonate.[59,60,61,62,63]

The presence of relatively heavy $\delta^{18}O_w$ values in the GCP is unsurprising when considering modern spatial patterns.[66,67] Modern surface water $\delta^{18}O_w$ values in the Gulf of

Mexico are heavier than the mean ocean by ~1.0‰ due to the downwelling arm of the Hadley cell driving strong evaporation in the region.[68] This phenomenon was very likely present in the Cretaceous,[69,70,71] and would have driven ^{18}O enrichment whether evaporation was weaker, stronger, or equal in strength to today. This effect could have been enhanced if the WIS retreated northward,[72,73,74,75,76] removing major sources of moisture and isotopically light water masses in the GCP (Brown et al., *in press*).[72,77,78,79,80] Together, this data and other recent Δ_{47} studies suggest that the GCP, south and central WIS, and other shallow, low-to-mid latitude marine environments were consistently and substantially isotopically heavier than -1‰—testing our understanding of $\delta^{18}O_w$ values in an "ice-free" world.

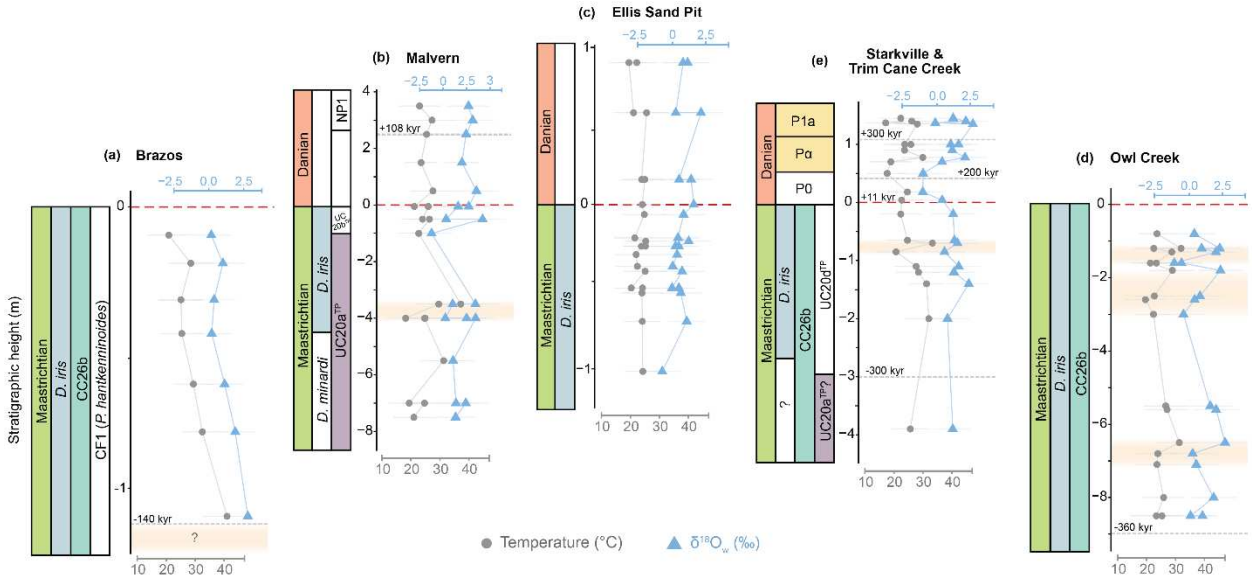


Figure 3. Temperature and $\delta^{18}O_w$ trends by site. Temperature data are represented by gray circles and trendlines and $\delta^{18}O_w$ data by blue triangles and trendlines. Each stratigraphic section has been aligned in height and centered around the K-Pg boundary (red dashed lines). Key biostratigraphic zones are color coordinated across panels to show equivalent temporal coverage. Potential warming intervals are highlighted in orange (see Results). Age constraints are given in estimated kyr before or after the K-Pg boundary (see section I of the supplemental text). Error bars in all other panels represent the 95% confidence interval calculated from long-term standard

reproducibility. Individual points represent the average of minimum three replicates (see Methods). We direct the reader to the supplemental material for detailed descriptions of lithology, age models, sample collection, and other characteristics of each site.

Maastrichtian temperature and $\delta^{18}O_w$ trends through time

The onset of Deccan Trap volcanism in the latest Maastrichtian represents a potentially global-scale environmental perturbation preceding the K-Pg.[28,29,81] The Deccan Traps eruptions lasted from ~400 kyr before to ~300 kyr after the K-Pg, and are largely understood to have caused global warming during the Late Maastrichtian Warming Event (LMWE) from 400 to 150 kyr before the boundary.[5,82,83,84,85] The LMWE has been identified globally in sites from the Atlantic coast of North America[86], northwest Europe and Russia,[87,88,89,90] the James Ross Basin, Antarctica,[91,92] western Texas,[93,94] and various deep-sea cores across multiple ocean basins.[82,95,96] In this study, three Maastrichtian sites (Starkville, Malvern, and the Owl Creek Type Section) contain or lie within the *Discoscaphites iris* Ammonite Range Zone (corresponding to the last ~400 kyr of the Cretaceous)[29,97] and therefore have the potential to record the LMWE (Fig. 3).[28,29,81]

While small sample sizes, depositional hiatuses, and variable sedimentation rates at each site complicate interpretation of temporal trends in the GCP, potential warming events can be suggested at a preliminary level (Fig. 3). At the Starkville site, there is warming of ~12 ˚C in the *D. iris* Zone, but this is based on only two samples. A larger number of samples (n = 5) at Malvern record a warming of ~11 ˚C during a similar temporal interval. At the Owl Creek Type Section, the coarse age model cannot identify which temperature peak (if any) is most likely representative of the LMWE, but multiple warming shifts of at least 6–7 ˚C are shown. We additionally suggest that the ~12 ˚C of cooling in the Brazos succession (n = 6), which was

deposited in the final 140 kyr of the Maastrichtian, could represent the decline from the LMWE. Taken together, these results suggest that the LMWE is present in the GCP and may have warmed the environment by at least 6 ˚C, although this value should be treated cautiously based on the limited sample sizes and associated uncertainties (Fig. 4a).

The degree of warming potentially observed during the LMWE in the GCP is greater than that derived from compilations of organic and inorganic proxies (~2 ˚C),[82] but aligns well with other Δ_{47} studies in Antarctica (~8 ˚C) and the Netherlands (6–9 ˚C; Fig. 4).[87,91] Our results demonstrate that $\delta^{18}O_w$ is variable with temperature (Fig. 3; see discussion below) and almost always heavier than the "ice-free" assumption of -1‰ (Fig. S14).[59,60,61] The use of a static $\delta^{18}O_w$ value can ultimately obfuscate paleotemperature patterns (Fig. 4a) and may explain why Δ_{47} records depict the LMWE as more intense and abrupt, while the $\delta^{18}O$ proxy produces a smaller, more gradual excursion.[82] Interestingly, benthic foraminifera—which would experience smaller fluctuations in $\delta^{18}O_w$ than surface dwellers—record 2–4 ˚C of warming in intermediate and deep water, indicating the viability of greater degrees of warming in surface waters.[98,99]

Our reconstructions at each site in the GCP illustrate that $\delta^{18}O_w$ is variable through time and directly mimics changes in temperature (Fig. 3; Figs. S12 and S13; Table S3). This has been observed in other paired Δ_{47} temperature and $\delta^{18}O_w$ records of the LMWE and K-Pg, although how this occurs in a world without polar ice caps remains a subject of speculation.[87,91,100] Petersen et al. (2016) attributed the temperature and $\delta^{18}O_w$ relationship in Antarctica to seasonal variation in continental runoff, while O'Hora et al. (2022) hypothesized that it was due to changes in dominant water masses in the basin or to the migration of precipitation bands in the modern day Maastricht region. Müller et al. (2026), who similarly measured the Δ_{47} of Late Maastrichtian macrofossils around Maastricht, again found that temperature and $\delta^{18}O_w$ covaried

through time and attributed this result to potential runoff, circulation, or evaporation and precipitation effects. Coupling of these parameters in the GCP, which occupies a very different climatic and oceanographic setting from Antarctica or northwest Europe, could be attributed to unique local factors like the closure of the WIS.[72,75] However, the multiple, global observations of this covariance may indicate a need for a universal mechanism driving variation in $\delta^{18}O_w$ during the LMWE, perhaps related to changes in the global hydrological cycle or continental water storage.[101]

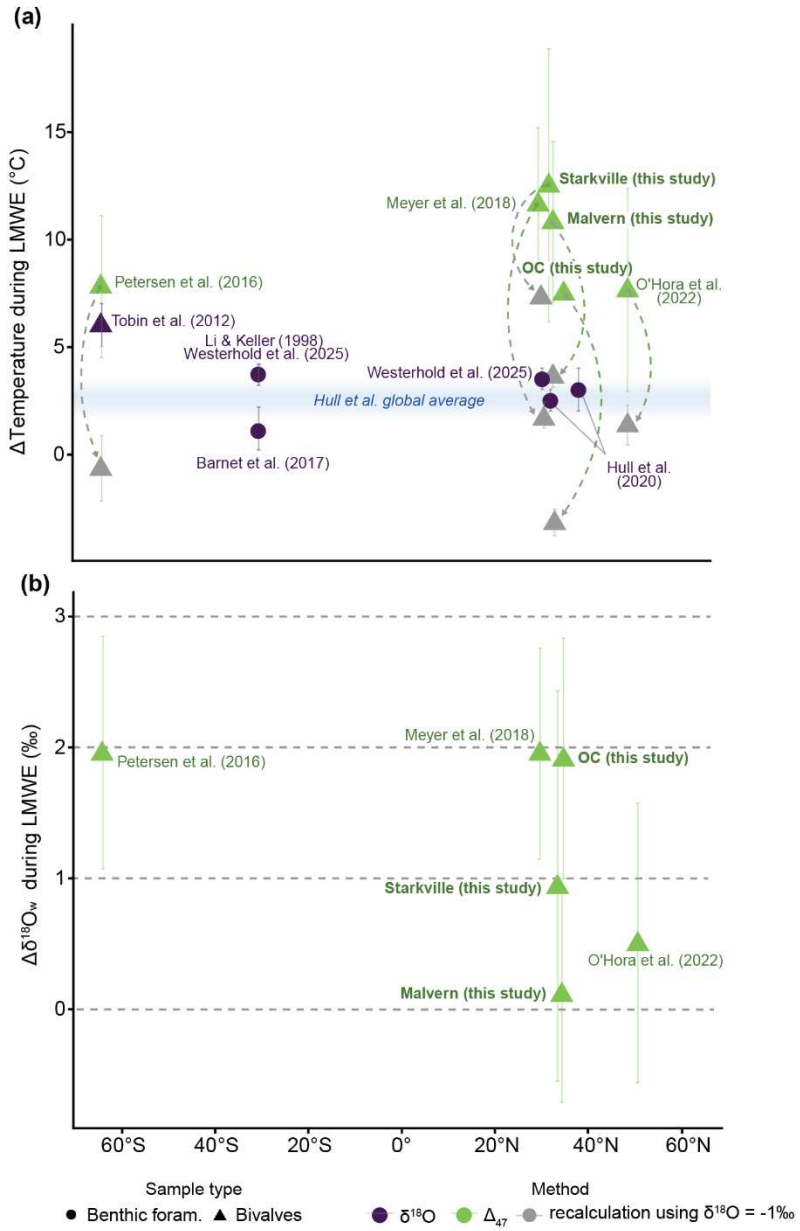


Figure 4. A compilation of temperature and $\delta^{18}O_w$ changes during the Late Maastrichtian Warming Event (LMWE) by latitude. In panel a), estimates of LMWE warming from Δ_{47} studies are given in green and from $\delta^{18}O$ in purple. The sample type is indicated by shape, where benthic foraminifera are circles and bivalves are triangles. The globally averaged warming reported in Hull et al. (2020) is highlighted in blue. The two other points from Hull et al. (2020) represent original data from the study from J-Anomaly Ridge and Hess Rise. Relative temperature changes during the LMWE reported from Δ_{47} studies have been recalculated using a $\delta^{18}O_w$ assumption of -1‰ (gray arrows leading to gray triangles). Panel b) summarizes the change in $\delta^{18}O_w$ during the LMWE. Error bars of previous $\delta^{18}O$ studies represent one sd or have been made to reflect reported ranges in text or figures. For all Δ_{47} studies and $\delta^{18}O_w$ = -1‰ recalculations, uncertainties were calculated by propagating the 95% confidence interval of individual samples from long-term reproducibility of standards.

Danian temperature trends through time

Danian temperature trends are, like the Maastrichtian, challenging to interpret due to unconstrained hiatuses between the impact event and the resumption of background deposition, variable sedimentation rates, and coarse age models. With these considerations, we provide evidence that Cretaceous-level warmth (i.e., temperatures of ~25 ˚C) returned to the GCP within ~100 kyr following the K-Pg boundary (Fig. 3). At the Malvern site, temperatures reached 25 ˚C within 108 kyr after the impact (Fig. 2). At Trim Cane Creek, where the age model is most tightly constrained using foraminiferal biostratigraphy, warm conditions are recorded by the lowest Danian samples, deposited between 3 and 11 kyr after the K-Pg.[102,103] Younger samples deposited 200–300 kyr post-impact sustain this warmth, but exhibit more variability. This variability is possibly the product of greater time-averaging within these horizons (refer to Supplemental Text). Despite poor age constraints in the Danian at Ellis Sand Pit, we again find that warm conditions returned following the K-Pg, although improved age models are required to determine the timescale over which this occurred.

We find our above timelines of shallow marine climate stabilization to be on the same orders of magnitude as those from previous studies.[82,104,105,106] Pickersgill et al. (2021) and Barnet et al. (2019) showed deep marine temperatures returning at 250,000 years post-impact based on the $\delta^{18}O$ values of benthic foraminifera. The planktonic $\delta^{18}O$ record presented in Gilabert et al. (2025) implies that oceanographic conditions returned to Maastrichtian levels between 10–50 kyr after the impact event and may be more analogous to our samples. A fast temperature stabilization has also been seen in terrestrial systems, where climate appeared to rebound quickly after the immediate disruption.[107,108] At a finer scale, previous studies of Danian temperature trends have reconstructed and modelled a year- to decadal-scale impact winter. During this event, sea surface temperatures may have decreased by 2–3 ˚C, based on TEX_{86}

269 records in the GCP and Atlantic Coast,[16,109] or by as much as ~15 ˚C as predicted by recent
270 global ecosystem models.[17] MacLeod et al. (2025) found a brief warming of ~5 ˚C after the
271 impact winter during the P0 planktonic foraminiferal zone (< 30,000 years post-impact) at the
272 Brazos locality,[15,16] but our methods (i.e., bulk sampling of macrofossils) and available age
273 models preclude potential observation of this event. Still, we offer evidence that the physical
274 climate of shallow marine environments in the GCP returned to pre-impact conditions on
275 geologically rapid (~10–100 kyr) time scales.

276 **DISCUSSION**

277 The end-Cretaceous is known for a series of major physical perturbations, with debate
278 persisting about the relative magnitude of biological, environmental, and climatic change
279 associated with each.[110] We find that regional temperatures and $\delta^{18}O_w$ were consistent between
280 the late Maastrichtian and early Danian (following any decadal-scale impact winter, which is not
281 observed here due to our sample coverage), indicating that the climate leading up to the impact
282 returned within ~10–100s of kyr afterward. This result implies that shallow marine ecosystems in
283 the GCP would experience the return of a similar climate if they could survive the extreme, but
284 geologically-brief, disruptions from the impact.[1,8,14]

285 Our Δ_{47} records further suggest that the LMWE is recorded in shallow marine successions
286 within the GCP and may be associated with greater amounts of warming (> 6 ˚C) than previously
287 proposed. Specifically, we find that $\delta^{18}O_w$ varies temporally and in phase with temperature at all
288 sites in the GCP—potentially masking the severity of the LMWE in $\delta^{18}O$-based records.
289 Furthermore, the Δ_{47} proxy, with a greater number of records, has the ability to better illustrate
290 climate sensitivity and global patterns of the Deccan Trap eruptions, especially compared to
291 events at the K-Pg boundary itself.[111,112,113,114]

In sum, our results provide new insights into the rebound of physical climate and drivers of ecosystem recovery and restructuring in shallow marine settings following the Chicxulub impact. Our data suggest that temperatures recovered on relatively rapid (~10 to 100 kyr) timescales to pre-extinction conditions across a range of shallow marine settings—even in areas proximal to the impact. Given the longer timelines of recovery for ecological systems,[19,21,115] physical climate change is therefore unlikely to have been a significant driver of long-term biotic responses following the K-Pg mass extinction. Rather, protracted Earth System recovery on the scale of 100 kyr to Myr was likely primarily controlled by biotic and ecological factors following trophic collapse, loss of ecosystem function, and complexity in the aftermath of the impact.

METHODS

Sample Collection

High-resolution stratigraphic sampling occurred across five states and eight localities in the GCP: Brazos (Texas), Malvern (Arkansas), Owl Creek Type Section (Mississippi), Ellis Sand Pit (Mississippi), Starkville (Mississippi), Trim Cane Creek (Mississippi), and Braggs (Alabama). Providence Sand Formation samples from the Walter F. George Reservoir (Georgia and Alabama) were obtained from the Sohl Collection in the Smithsonian National Museum of Natural History's Department of Paleobiology. Brazos samples were previously published in Brown et al. (in review). All sites contain Maastrichtian deposits, and three contain Danian (Malvern, Ellis Sand Pit, and Starkville). Detailed descriptions of the samples, stratigraphy, lithology, and age models for each site can be found in the supplementary text.

The majority of samples were epifaunal oysters (n = 75), with the remainder being infaunal clams (n = 37), semi-infaunal gastropods (n = 2), and infaunal scallops (n = 2).

Common genera include *Gryphaeostrea*, *Ostrea*, *Exogyra*, *Anomia*, *Corbula*, *Crassatella*, *Nucula*, and *Nuculana*, with six samples being unidentified bivalves. Most samples were calcitic mineralogies (all oysters, scallops, and clams of the genus *Anomia*; n = 84), with all other clams and gastropods primarily composed of aragonite (n = 41). For all sample metadata, refer to the supplemental text and tables.

Sample preservation screening

Shell preservation was first assessed using scanning electron microscopy (SEM) to ensure original mineralogy and shell microstructures were intact. Shells with sufficient material (n = 53) were gold sputter coated using a Denton Desk II for 90 s and secured on angled aluminum SEM mounts using conductive carbon adhesive. A cross-section of each shell was imaged using a JEOL JSM-7800FLV field-emission scanning electron microscope. Images were taken at progressively increasing magnification, with the most holistic views available in the range of 1500-3000x magnification. A two-part ranking system[87] was used to quantify the extent of dissolution and secondary material in each sample, where each was assigned a value representing the extent between 0 (none) to 3 (extensive). A sample was determined to be well-preserved and included in the above results only if there was no or minimal secondary growth (≤ 1). All but two samples demonstrated excellent preservation under the SEM (Fig. S10).

We then measured trace element concentrations of the specimens, as high concentrations of iron (Fe) and/or manganese (Mn) have been previously used to detect diagenetic alteration of carbonates from meteoric fluids.[87,116,117,118,119] To prepare specimens for trace element analysis, sediment was brushed from the surface and then the carbonate carefully sampled using a hand drill on low speeds (1000 rpm) and with short (< 1 s) touches to avoid frictional heating. Shells

that were too thin to drill (< 1 mm) were crushed into a uniform powder using a mortar and pestle.

Nearly all samples in the dataset (n = 99) were analyzed for trace elements. Samples were run on the Thermo iCAP ICP-OES 7400 Duo in the PACE lab at the University of Michigan, following methods described in Dyez et al. (2024). A small number (n = 3) of samples had extremely high Fe concentrations (> 15,000 ppm) and were removed as outliers from the final dataset. The remaining samples were assessed within each site to account for spatial heterogeneity in baseline Fe or Mn concentrations (Fig. S9). Using this approach, a total of nine outliers were removed from six sites. All removed samples and rationale can be found in the Supplemental Spreadsheet.

Isotopic Analysis

Shells were sampled for a minimum of 12 mg of material using the same method of drilling as described above. A minimum of three replicates of each sample were simultaneously analyzed for $\delta^{18}O$, $\delta^{13}C$, and $\Delta_{47–48}$ in the Stable and Clumped Isotopes for Paleoclimate and Paleoceanography (SCIPP) Lab at the University of Michigan. All measurements were made on a Nu Perspective isotope dual-inlet ratio mass spectrometer with an attached NuCarb automated sample preparation device—identical to methods described in O'Hora et al. (2022), Zhang and Petersen (2023), and Hoffman et al. (2025). Briefly, individual sample aliquots were reacted with phosphoric acid at 70 ˚C. Released CO_2 was then purified using a series of water and polymer absorbent traps. Samples with sufficient material (> 3 mg per replicate) were analyzed in 'bellows mode' (n = 101), while the remaining samples were run in 'cold finger mode' (n = 10); a method that allows very small amounts of CO_2 to be analyzed by freezing gas into a cold finger

adjacent to the change-over block.[87,120,121] CO_2 was then analyzed at a current of 80nA over 80 ('bellows mode') or 60 ('cold finger mode') sample-reference cycles.

Isotope ratios were calculated using the ^{17}O parameters presented in Brand et al. (2010) and processed in R using scripts from Petersen et al. (2019). Δ_{47} values were corrected relative to the Intercarb-Carbon Dioxide Equilibrium Scale (I-CDES) reference frame using the ETH 1–4 standards.[49] Δ_{48} values were corrected using a fixed offset from two in-house standards[122] and converted to the GU-CDES reference frame based on the GU1 standard.[52,123]

Paleotemperature calculations

Δ_{47}-derived temperatures were calculated using the calibration of Anderson et al. (2021) given in Eq. 1:

$$\Delta_{47\ (I-CDES)} = 0.0391 \pm 0.0004 \times \frac{10^6}{T^2} + 0.154 \pm 0.004 \quad (1)$$

where T is temperature in Kelvin. $\delta^{18}O_w$ values were calculated following the calcite-water relationship (Eq. 2) in Kim and O'Neil (1997) or the aragonite-water relationship in Kim et al. (2007; Eq. 3):

$$1000\ln\alpha_{(calcite-H_2O)} = 18.03 \times \frac{10^3}{T} - 32.42 \quad (2)$$

$$1000\ln\alpha_{(aragonite-H_2O)} = 17.88 \times \frac{10^3}{T} - 31.46 \quad (3)$$

where α is the fractionation factor between the $CaCO_3$ phase and water and T is temperature in Kelvin. For comparisons to other published calibrations, see Fig. S14 and Table S4.

Statistics and reproducibility

Long-term reproducibility (1 sd) remained at ≤ 0.017‰ for Δ_{47} and ≤ 0.091‰ for Δ_{48} during all analytical sessions. Using these values, we report the 95% confidence interval (CI) for each sample temperature and $\delta^{18}O_w$, as well as the standard error based on a minimum of three

replicates. When we discuss binned averages, such as that for a specific stage or site, we report the 95% CI of the mean of all replicated sample measurements in the bin.

When comparing two populations (e.g., temperature between the Maastrichtian and Danian) or a population against a known value (e.g., reconstructed $\delta^{18}O_w$ values relative to -1‰) we report p-values generated by Welch's t-tests. When comparing multiple populations (used in comparisons between environments), we used a one-way Welch's ANOVA test followed by a Games-Howell post-hoc test. Tests were chosen for their ability to handle differing sample sizes and variances between populations. Normality of the data was assessed using histograms, Q-Q plots, and Shapiro-Wilk tests.

DATA AVAILABILITY

All data generated or analyzed during this study are included in this published article and its supplementary information files. The data will be made available in the EarthChem repository upon publication.

ACKNOWLEDGEMENTS

The authors would like to thank George Phillips (Mississippi Museum of Natural Sciences) and Carson Sloan (Arkansas Department of Transportation) for assisting with access to localities and useful discussions, and landowners in Texas (Ronnie and Jackie Mullinax), Mississippi (Allan and Betty Carrol and Charlie Gardner), and Alabama who provided access to their properties for sampling. We also acknowledge Justin VanDeVelde for overseeing clumped isotope analyses, Owen Neil for assistance with SEM operations, and Kelsey Dyez for running elemental analyses, as well as all students and scientists associated with NSF grant #1924807 (CM). This work was funded by the University of New Mexico Postdoctoral Fellowship (JW), the University of Michigan Scott Turner Award (AB), and NSF-OCE-2037752 (CL and LK). The

funders played no role in study design, data collection, analysis and interpretation of data, or the writing of this manuscript.

AUTHOR INFORMATION

Department of Earth and Environmental Sciences, University of Michigan, Ann Arbor, Michigan, U.S.A

Adriana Brown, Sierra Petersen & Jonathan Hoffman-Vinje

Department of Biological and Environmental Engineering, Cornell University, Ithaca, NY U.S.A.

Samantha Davies

Natural History Museum, London, Great Britain

James Witts

Department of Earth and Planetary Sciences, University of New Mexico, Albuquerque, New Mexico, U.S.A

Corinne Myers & Jone Naujokaityte

Geology Department, San José State University, San José, California, U.S.A.

Carlie Pietsch

Department of Earth and Environmental Sciences, Brooklyn College, City University of New York, Brooklyn, New York, U.S.A.

Matthew Garb

Division of Paleontology, American Museum of Natural History, New York City, New York, U.S.A.

Neil Landman

Department of Earth Sciences, University College London, London, United Kingdom

Paul Bown

Institute for Geophysics, Department of Earth and Planetary Sciences, University of Texas at Austin, Austin, Texas, U.S.A.

Christopher Lowery, Lorna Kearns

AUTHOR CONTRIBUTIONS

AB, SD, SP, JW, CM, and CP were involved in project conceptualization. AB, SD, JW, PB, CL, LK and JH performed analyses and data collection. Samples were collected through multiple field campaigns by SD, SP, JW, CM, CP, JN, and CL. AB, SD, SP, JW, CM, CP, and JN led work on the initial drafts of this manuscript and all other authors participated in later stages of editing. All authors read and approved the final manuscript.

COMPETING INTERESTS

All authors declare no financial or non-financial competing interests.

REFERENCES

[1] Gulick, S. P. S. End of the Cretaceous. in *Cretaceous Project 200 Volume 1: The Cretaceous World* (eds Hart, M. B. et al.) SP544-2023-176 (Geological Society of London, 2025).

[2] Hildebrand, A. R. *et al.* Chicxulub Crater – a possible Cretaceous Tertiary boundary impact crater on the Yucatan Peninsula, Mexico. *Geology* **19**, 867–871 (1991).

[3] Alvarez, L. W., Alvarez, W., Asaro, F. & Michel, H. V. Extraterrestrial cause for the Cretaceous-Tertiary extinction. *Science* **208**, 1095–1108 (1980).

[4] Schulte, P. *et al.* The Chicxulub asteroid impact and mass extinction at the Cretaceous-Paleogene boundary. *Science* **327**, 1214–1218 (2010).

[5] Renne, P. R. *et al.* Time scales of critical events around the Cretaceous-Paleogene boundary. *Science* **339**, 684–687 (2013).

[6] Bambach, R. K. Phanerozoic biodiversity mass extinctions. *Annu. Rev. Earth Planet. Sci.* **34**, 127–155 (2006).

[7] Range, M. M. *et al.* The Chicxulub impact produced a powerful global tsunami. *AGU Adv.* **3**, e2021AV000627 (2022).

[8] Morgan, J. V., Bralower, T. J., Brugger, J. & Wünnemann, K. The Chicxulub impact and its environmental consequences. *Nat. Rev. Earth Environ.* **3**, 338–354 (2022).

[9] Kinsland, G. L., Egedahl, K., Strong, M. A. & Ivy, R. Chicxulub impact tsunami megaripples in the subsurface of Louisiana: Imaged in petroleum industry seismic data. *Earth Planet. Sci. Lett.* **570**, 117063 (2021).

[10] Day, S. & Maslin, M. Linking large impacts, gas hydrates, and carbon isotope excursions through widespread sediment liquefaction and continental slope failure: The example of the KT boundary event. in *Impacts, Rocks and Ecology* (eds Koeberl, C. & MacLeod, K. G.) 239–258 (Geological Society of America, 2005).

[11] Kring, D. A. & Durda, D. D. Trajectories and distribution of material ejected from the Chicxulub impact crater: Implications for postimpact wildfires. *J. Geophys. Res. Planets* **107**, 6–1 (2002).

[12] Krogh, T. E., Kamo, S. L., Sharpton, V. L., Marin, L. E. & Hildebrand, A. R. U–Pb ages of single shocked zircons linking distal K/T ejecta to the Chicxulub crater. *Nature* **366**, 731–734 (1993).

[13] Henehan, M. J. *et al.* Rapid ocean acidification and protracted Earth system recovery followed the end-Cretaceous Chicxulub impact. *Proc. Natl. Acad. Sci. USA* **116**, 22500–22504 (2019).

[14] Senel, C. B. *et al.* Chicxulub impact winter sustained by fine silicate dust. *Nat. Geosci.* **16**, 1033–1040 (2023).

[15] MacLeod, K. G. *et al.* Isotopic evidence from a Brazos River (Texas, USA) Cretaceous/Paleogene boundary section consistent with a pulse of greenhouse warming shortly after the Chicxulub impact. *Glob. Planet. Change* **253**, 104924 (2025).

[16] Vellekoop, J. *et al.* Rapid short-term cooling following the Chicxulub impact at the Cretaceous–Paleogene boundary. *Proc. Natl. Acad. Sci. USA* **111**, 7537–7541 (2014).

[17] Ying, R., Monteiro, F. M., Witts, J. D. & Schmidt, D. N. Darkness and body size shaped end-Cretaceous marine extinction patterns. *Nature* **649**, 1–6 (2026).

[18] Bown, P. Selective calcareous nannoplankton survivorship at the Cretaceous-Tertiary boundary. *Geology* **33**, 653–656 (2005).

[19] Sosa Montes de Oca, C. *et al.* Intense changes in the main source of organic carbon to the Gulf Coastal Plain following the Cretaceous-Paleogene boundary. *Paleoceanogr. Paleoclimatol.* **39**, e2024PA004887 (2024).

[20] Lowery, C. M. & Bralower, T. J. Elevated post K-Pg export productivity in the Gulf of Mexico and Caribbean. *Paleoceanogr. Paleoclimatol.* **37**, e2021PA004400 (2022).

[21] Birch, H. S., Coxall, H. K., Pearson, P. N., Kroon, D. & Schmidt, D. N. Partial collapse of the marine carbon pump after the Cretaceous-Paleogene boundary. *Geology* **44**, 287–290 (2016).

[22] Pindell, J. & Kennan, L. Tectonic evolution of the Gulf of Mexico, Caribbean and northern South America in the mantle reference frame: An update. in *The Geology and Evolution of the Region Between North and South America* (eds James, K., Lorente, M. & Pindell, J.) **328**, 1–55 (Geological Society of London, 2009).

[23] Anderson, T. & Schmidt, V. The evolution of Middle America and the Gulf of Mexico Caribbean Sea region during Mesozoic time. *Geol. Soc. Am. Bull.* **94**, 941–966 (1983).

[24] Claeys, P., Kiessling, W. & Alvarez, W. Distribution of Chicxulub ejecta at the Cretaceous-Tertiary boundary. in *Catastrophic Events and Mass Extinctions: Impacts and Beyond* (eds Koeberl, C. & MacLeod, K. G.) 55–68 (Geological Society of America, 2002).

[25] Mancini, E., Puckett, T. & Tew, B. Integrated biostratigraphic and sequence stratigraphic framework for Upper Cretaceous strata of the eastern Gulf Coastal Plain, USA. *Cretaceous Res.* **17**, 645–669 (1996).

[26] Puckett, T. Integrated event stratigraphic framework of the marine Upper Cretaceous (Santonian-Maastrichtian) deposits of the eastern Mississippi Embayment, USA. *Geol. Soc. Am. Bull.* **138**, 299–341 (2026).

[27] Witts, J. D. *et al.* Cephalopods from the Cretaceous-Paleogene (K-Pg) boundary interval on the Brazos River, Texas, and extinction of the ammonites. *Am. Mus. Novit.* **2020** (3964), 1–52 (2021).

[28] Witts, J. D. *et al.* A fossiliferous spherule-rich bed at the Cretaceous–Paleogene (K–Pg) boundary in Mississippi, USA: Implications for the K–Pg mass extinction event in the Mississippi Embayment and Eastern Gulf Coastal Plain. *Cretaceous Res.* **91**, 147–167 (2018).

[29] Larina, E. *et al.* Upper Maastrichtian ammonite biostratigraphy of the Gulf Coastal Plain (Mississippi Embayment, southern USA). *Cretaceous Res.* **60**, 128–151 (2016).

[30] Dastas, N. R., Chamberlain, J. A. & Garb, M. P. Cretaceous-Paleogene dinoflagellate biostratigraphy and the age of the Clayton Formation, Southeastern Missouri, USA. *Geosciences* **4**, 1–29 (2014).

[31] Keller, G., Abramovich, S., Adatte, T. & Berner, Z. Biostratigraphy, age of Chicxulub impact, and depositional environment of the Brazos River KTB sequences. in *The End-Cretaceous Mass Extinction and the Chicxulub Impact in Texas* (eds Keller, G. & Adatte, T.) **100**, 82–122 (SEPM Society for Sedimentary Geology, 2011).

[32] Irizarry, K. *et al.* Faunal and stratigraphic analysis of the basal Cretaceous-Paleogene (K-Pg) boundary event deposits, Brazos River, Texas, USA. *Palaeogeogr. Palaeoclimatol. Palaeoecol.* **610**, 111340 (2023).

[33] Lowery, C. M., Kaskes, P., Witts, J. D. & Pietsch, C. Exploring the K/Pg boundary in central Texas: Brazos River outcrops and the Gulf Coast Core Repository. in *From Orogenies to Hydrology: Geologic Excursions in Texas and Beyond* (eds Fleming, Z. & Cannon, J.) **74**, 17–44 (Geological Society of America, 2025).

[34] Donovan, A. D. *et al.* Sequence stratigraphic setting of the Cretaceous-Tertiary boundary in central Alabama. *SEPM Spec. Publ.* **42**, 299–307 (1988).

[35] Sessa, J. A. *et al.* Ammonite habitat revealed via isotopic composition and comparisons with co-occurring benthic and planktonic organisms. *Proc. Natl. Acad. Sci. USA* **112**, 15562–15567 (2015).

[36] Sessa, J. A., Bralower, T. J., Patzkowsky, M. E., Handley, J. C. & Ivany, L. C. Environmental and biological controls on the diversity and ecology of Late Cretaceous through early Paleogene marine ecosystems in the U.S. Gulf Coastal Plain. *Paleobiology* **38**, 218–239 (2012).

[37] Vellekoop, J. *et al.* Shelf hypoxia in response to global warming after the Cretaceous-Paleogene boundary impact. *Geology* **46**, 683–686 (2018).

[38] Hart, M. B., Harries, P. J. & Cárdenas, A. L. The Cretaceous/Paleogene boundary events in the Gulf Coast: Comparisons between Alabama and Texas. *GCAGS Trans.* **63**, 235–256 (2013).

[39] Eiler, J. M. "Clumped-isotope" geochemistry—The study of naturally-occurring, multiply-substituted isotopologues. *Earth Planet. Sci. Lett.* **262**, 309–327 (2007).

[40] Eiler, J. M. Paleoclimate reconstruction using carbonate clumped isotope thermometry. *Quat. Sci. Rev.* **30**, 3575–3588 (2011).

[41] Ghosh, P. *et al.* 13C–18O bonds in carbonate minerals: A new kind of paleothermometer. *Geochim. Cosmochim. Acta* **70**, 1439–1456 (2006).

[42] Huntington, K. W. & Petersen, S. V. Frontiers of carbonate clumped isotope thermometry. *Annu. Rev. Earth Planet. Sci.* **51**, 611–641 (2023).

[43] Kennett, J. P. & Shackleton, N. J. Oxygen isotopic evidence for the development of the psychrosphere 38 Myr ago. *Nature* **260**, 513–515 (1976).

[44] Jones, L. A., Dean, C. D., Gearty, W. & Allen, B. J. rmacrostrat: An R package for accessing and retrieving data from the Macrostrat geological database. *Geosphere* **20**, 1456–1467 (2024).

[45] Garrity, C. & Soller, D. Database of the Geologic Map of North America—Adapted from the map by J.C. Reed, Jr. and others (2005). *USGS Data Ser.* **424** (2009).

[46] King, D. T., Jr. & Skotnicki, M. C. Sedimentary facies, sea level history, and paleogeography of the Upper Cretaceous (Maastrichtian) Providence Sand, central and eastern Coastal Plain of Alabama. *Ala. Geol. Surv. Bull.* **140**, 1–55 (1991).

[47] Meyer, K. W., Petersen, S. V., Lohmann, K. C. & Winkelstern, I. Z. Climate of the Late Cretaceous North American Gulf and Atlantic Coasts. *Cretaceous Res.* **89**, 160–173 (2018).

[48] Jones, M. M., Petersen, S. V. & Curley, A. N. A tropically hot mid-Cretaceous North American Western Interior Seaway. *Geology* **50**, 954–958 (2022).

[49] Bernasconi, S. M. *et al.* InterCarb: A community effort to improve interlaboratory standardization of the carbonate clumped isotope thermometer using carbonate standards. *Geochem. Geophys. Geosyst.* **22**, e2020GC009588 (2021).

[50] Anderson, N. T. *et al.* A unified clumped isotope thermometer calibration (0.5–1,100°C) using carbonate-based standardization. *Geophys. Res. Lett.* **48**, e2020GL092069 (2021).

[51] Petersen, S. V. *et al.* Effects of improved 17O correction on interlaboratory agreement in clumped isotope calibrations, estimates of mineral-specific offsets, and temperature dependence of acid digestion fractionation. *Geochem. Geophys. Geosyst.* **20**, 3495–3519 (2019).

[52] Fiebig, J. *et al.* Carbonate clumped isotope values compromised by nitrate-derived NO2 interferent. *Chem. Geol.* **670**, 122382 (2024).

[53] Linnert, C. *et al.* Evidence for global cooling in the Late Cretaceous. *Nat. Commun.* **5**, 4194 (2014).

[54] O'Brien, C. L. *et al.* Cretaceous sea-surface temperature evolution: Constraints from TEX86 and planktonic foraminiferal oxygen isotopes. *Earth-Sci. Rev.* **172**, 224–247 (2017).

[55] Hollis, C. J. *et al.* Early Paleogene temperature history of the Southwest Pacific Ocean: Reconciling proxies and models. *Earth Planet. Sci. Lett.* **349–350**, 53–66 (2012).

[56] Steinig, S. *et al.* Evidence for a regional warm bias in the Early Cretaceous TEX86 record. *Earth Planet. Sci. Lett.* **539**, 116184 (2020).

[57] Inglis, G. N. & Tierney, J. E. *The TEX86 Paleotemperature Proxy* (Cambridge University Press, 2020).

[58] Zachos, J. C., Arthur, M. A. & Dean, W. E. Geochemical and paleoenvironmental variations across the Cretaceous/Tertiary boundary at Braggs, Alabama. *Palaeogeogr. Palaeoclimatol. Palaeoecol.* **69**, 245–266 (1989).

[59] Kim, S.-T. & O'Neil, J. R. Equilibrium and nonequilibrium oxygen isotope effects in synthetic carbonates. *Geochim. Cosmochim. Acta* **61**, 3461–3475 (1997).

[60] Grossman, E. L. & Ku, T.-L. Oxygen and carbon isotope fractionation in biogenic aragonite: Temperature effects. *Chem. Geol. Isot. Geosci. Sect.* **59**, 59–74 (1986).

[61] Kim, S.-T., O'Neil, J. R., Hillaire-Marcel, C. & Mucci, A. Oxygen isotope fractionation between synthetic aragonite and water: Influence of temperature and Mg2+ concentration. *Geochim. Cosmochim. Acta* **71**, 4704–4715 (2007).

[62] Grossman, E. L. Applying oxygen isotope paleothermometry in deep time. *Paleontol. Soc. Pap.* **18**, 39–68 (2012).

[63] Bemis, B. E., Spero, H. J., Bijma, J. & Lea, D. W. Reevaluation of the oxygen isotopic composition of planktonic foraminifera: Experimental results and revised paleotemperature equations. *Paleoceanography* **13**, 150–160 (1998).

[64] Daëron, M. *et al.* Most Earth-surface calcites precipitate out of isotopic equilibrium. *Nat. Commun.* **10**, 429 (2019).

[65] Dettman, D. L., Reische, A. K. & Lohmann, K. C. Controls on the stable isotope composition of seasonal growth bands in aragonitic fresh-water bivalves (Unionidae). *Geochim. Cosmochim. Acta* **63**, 1049–1057 (1999).

[66] Quizon, A. A., Gomes, L. D., Petersen, S. V. & VanDeVelde, J. Seawater salinity and oxygen isotopes along the U.S. East Coast from 24 °N to 44 °N. *Sci. Data* **13**, 7440 (2026).

[67] LeGrande, A. N. & Schmidt, G. A. Global gridded data set of the oxygen isotopic composition in seawater. *Geophys. Res. Lett.* **33**, L12604 (2006).

[68] Wagner, A. J. & Slowey, N. C. Oxygen isotopes in seawater from the Texas-Louisiana Shelf. *Bull. Mar. Sci.* **87**, 1–12 (2011).

[69] Hay, W. W. & DeConto, R. M. Comparison of modern and Late Cretaceous meridional energy transport and oceanology. in *Evolution of the Cretaceous Ocean-Climate System* (eds Barrera, E. & Johnson, C. C.) **332**, 283–300 (Geological Society of America, 1999).

[70] Hasegawa, H. *et al.* Drastic shrinking of the Hadley circulation during the mid-Cretaceous Supergreenhouse. *Clim. Past* **8**, 1323–1337 (2012).

[71] Zhang, S. *et al.* Variations of the Hadley circulation in the past 250 million years. *Atmos. Ocean. Sci. Lett.* **19**, 100851 (2026).

[72] Kauffman, E. G. & Caldwell, W. G. E. The Western Interior Basin in space and time. *Geol. Assoc. Can. Spec. Pap.* **39**, 1–30 (1993).

[73] Scotese, C. R., Vérard, C., Burgener, L., Elling, R. P. & Kocsis, A. T. The Cretaceous world: Plate tectonics, palaeogeography and palaeoclimate. *Geol. Soc. Lond. Spec. Publ.* **544**, SP544-2024–28 (2025).

[74] Slattery, J. S., Cobban, W. A., McKinney, K. C., Harries, P. J. & Sandness, A. L. Early Cretaceous to Paleocene paleogeography of the Western Interior Seaway: The interaction of eustasy and tectonism. *Wyo. Geol. Assoc. Field Conf. Guideb.* **68**, 22–60 (2013).

[75] Schueth, J. D., Wroblewski, A. & Minor, K. P. Revised paleogeographic maps of the North American Western Interior Seaway: Applying integrated approaches for predictive reconstructions and recognizing bias from lack of data. *AAPG Bull.* **109**, 991–1025 (2025).

[76] Cobban, W. A., Merewether, E. A., Fouch, T. D. & Obradovich, J. D. Some Cretaceous shorelines in the Western Interior of the United States. in *Mesozoic Systems of the Rocky Mountain Region, USA* (eds Caputo, M. V., Peterson, J. A. & Franczyk, K. J.) 393–414 (Rocky Mountain Section, SEPM, 1994).

[77] Wright, E. K. Stratification and paleocirculation of the Late Cretaceous Western Interior Seaway of North America. *Geol. Soc. Am. Bull.* **99**, 480–490 (1987).

[78] Hay, W. W., Eicher, D. L. & Diner, R. Physical oceanography and water masses in the Cretaceous Western Interior Seaway. *Geol. Assoc. Can. Spec. Pap.* **39**, 297–318 (1993).

[79] Fricke, H. C., Foreman, B. Z. & Sewall, J. O. Integrated climate model-oxygen isotope evidence for a North American monsoon during the Late Cretaceous. *Earth Planet. Sci. Lett.* **289**, 11–21 (2010).

[80] Curley, A. N., Petersen, S. V., Fricke, H. & Gleason, J. Insight into climate and hydrology of the late cretaceous western interior basin from clumped isotope paleothermometry and strontium isotopes. *Earth Planet. Sci. Lett.* **651**, 119180 (2025).

[81] Naujokaitytė, J. *et al.* Milankovitch cyclicity in the latest Cretaceous of the Gulf Coastal Plain, USA. *Sediment. Geol.* **421**, 105954 (2021).

[82] Hull, P. M. *et al.* On impact and volcanism across the Cretaceous-Paleogene boundary. *Science* **367**, 266–272 (2020).

[83] Sprain, C. J. *et al.* The eruptive tempo of Deccan volcanism in relation to the Cretaceous-Paleogene boundary. *Science* **363**, 866–870 (2019).

[84] Schoene, B. *et al.* U-Pb constraints on pulsed eruption of the Deccan Traps across the end-Cretaceous mass extinction. *Science* **363**, 862–866 (2019).

[85] Barnet, J. S. K. *et al.* A new high-resolution chronology for the late Maastrichtian warming event: Establishing robust temporal links with the onset of Deccan volcanism. *Geology* **46**, 147–150 (2017).

[86] Vellekoop, J., Woelders, L., Sluijs, A., Miller, K. G. & Speijer, R. P. Phytoplankton community disruption caused by latest Cretaceous global warming. *Biogeosciences* **16**, 4201–4210 (2019).

[87] O'Hora, H. E., Petersen, S. V., Vellekoop, J., Jones, M. M. & Scholz, S. R. Clumped-isotope-derived climate trends leading up to the end-Cretaceous mass extinction in northwestern Europe. *Clim. Past* **18**, 1963–1982 (2022).

[88] Sheldon, E., Ineson, J. & Bown, P. Late Maastrichtian warming in the Boreal Realm: Calcareous nannofossil evidence from Denmark. *Palaeogeogr. Palaeoclimatol. Palaeoecol.* **295**, 55–75 (2010).

[89] Thibault, N. *et al.* Upper Campanian–Maastrichtian chronostratigraphy of the Skælskør-1 core, Denmark: Correlation at the basinal and global scale and implications for changes in sea-surface temperatures. *Lethaia* **48**, 549–560 (2015).

[90] Ovechkina, M. N. & Alekseev, A. S. Quantitative changes of calcareous nannoflora in the Saratov region (Russian Platform) during the late Maastrichtian warming event. *J. Iberian Geol.* **31**, 149–165 (2005).

673 [91] Petersen, S. V., Dutton, A. & Lohmann, K. C. End-Cretaceous extinction in Antarctica
674 linked to both Deccan volcanism and meteorite impact via climate change. *Nat. Commun.*
675 **7**, 12079 (2016).

676 [92] Tobin, T. S. *et al.* Extinction patterns, δ18O trends, and magnetostratigraphy from a
677 southern high-latitude Cretaceous–Paleogene section: Links with Deccan volcanism.
678 *Palaeogeogr. Palaeoclimatol. Palaeoecol.* **350–352**, 180–188 (2012).

679 [93] Nordt, L., Atchley, S. & Dworkin, S. Terrestrial evidence for two greenhouse events in the
680 latest Cretaceous. *GSA Today* **13**, 4–9 (2003).

681 [94] Lesko, A., Dworkin, S. & Atchley, S. Terrestrial response to Maastrichtian climate change
682 determined from paleosols of the Dawson Creek Section, Big Bend National Park, Texas.
683 *Geosciences* **15**, 119 (2025).

684 [95] Keller, G., Punekar, J. & Mateo, P. Upheavals during the Late Maastrichtian: Volcanism,
685 climate and faunal events preceding the end-Cretaceous mass extinction. *Palaeogeogr.*
686 *Palaeoclimatol. Palaeoecol.* **441**, 137–151 (2016).

687 [96] Thibault, N. & Gardin, S. The late Maastrichtian nannofossil record of climate change in the
688 South Atlantic DSDP Hole 525A. *Mar. Micropaleontol.* **65**, 163–184 (2007).

689 [97] Landman, N. H., Johnson, R. O. & Edwards, L. E. Cephalopods from the
690 Cretaceous/Tertiary boundary interval on the Atlantic Coastal Plain, with a description of
691 the highest ammonite zones in North America. Part 2. Northeastern Monmouth County,
692 New Jersey. *Bull. Am. Mus. Nat. Hist.* **287**, 1–107 (2004).

693 [98] Westerhold, T. *et al.* Earth orbital rhythms links timing of Deccan trap volcanism phases
694 and global climate change. *Sci. Adv.* **11**, eadr8584 (2025).

695 [99] Li, L. & Keller, G. Abrupt deep-sea warming at the end of the Cretaceous. *Geology* **26**,
696 995–998 (1998).

697 [100] Müller, I. A. *et al.* Seawater properties based on clumped isotope analyses of macrofossil
698 assemblages from the Upper Cretaceous–lower Paleocene Type-Maastrichtian area.
699 *Cretaceous Res.* **179**, 106258 (2026).

700 [101] Sames, B., Wagreich, M., Conrad, C. P. & Iqbal, S. Aquifer-eustasy as the main driver of
701 short-term sea-level fluctuations during Cretaceous hothouse climate phases. *Geol. Soc.*
702 *Lond. Spec. Publ.* **498**, 9–38 (2020).

703 [102] Lowery, C. M. *et al.* Rapid recovery of life at Ground Zero of the end Cretaceous mass
704 extinction. *Nature* **558**, 288–291 (2018).

705 [103] Lowery, C. M., Bralower, T. J., Farley, K. & Leckie, R. M. New species evolved within a
706 few thousand years of the Chicxulub Impact. *Geology* **54**, 285–288 (2026).

707 [104] Pickersgill, A. E., Mark, D. F., Lee, M. R., Kelley, S. P. & Jolley, D. W. The Boltysh
708 impact structure: An early Danian impact event during recovery from the K-Pg mass
709 extinction. *Sci. Adv.* **7**, eabe6530 (2021).

710 [105] Barnet, J. S. K. *et al.* A high-fidelity benthic stable isotope record of Late Cretaceous–
711 Early Eocene climate change and carbon-cycling. *Paleoceanogr. Paleoclimatol.* **34**, 672–
712 691 (2019).

[106] Gilabert, V. *et al.* Evaluation of the main drivers of environmental and climatic changes of the sea-surface across the Cretaceous-Paleogene transition: A global perspective. *Geobios* **88–89**, 125–137 (2025).

[107] Zhang, L. *et al.* Deccan volcanism caused coupled pCO2 and terrestrial temperature rises, and pre-impact extinctions in northern China. *Geology* **46**, 271–274 (2018).

[108] Dzombak, R. M., Sheldon, N. D., Mohabey, D. M. & Samant, B. Stable climate in India during Deccan volcanism suggests limited influence on K–Pg extinction. *Gondwana Res.* **85**, 19–31 (2020).

[109] Vellekoop, J. *et al.* Evidence for Cretaceous-Paleogene boundary bolide "impact winter" conditions from New Jersey, USA. *Geology* **44**, 619–622 (2016).

[110] Henehan, M. J., Hull, P. M., Penman, D. E., Rae, J. W. B. & Schmidt, D. N. Biogeochemical significance of pelagic ecosystem function: An end-Cretaceous case study. *Philos. Trans. R. Soc. B Biol. Sci.* **371**, 20150510 (2016).

[111] He, H., Kramer, R. J., Soden, B. J. & Jeevanjee, N. State dependence of CO2 forcing and its implications for climate sensitivity. *Science* **382**, 1051–1056 (2023).

[112] Meraner, K., Mauritsen, T. & Voigt, A. Robust increase in equilibrium climate sensitivity under global warming. *Geophys. Res. Lett.* **40**, 5944–5948 (2013).

[113] Held, I. M. & Soden, B. J. Robust responses of the hydrological cycle to global warming. *J. Clim.* **19**, 5686–5699 (2006).

[114] Wu, P., Christidis, N. & Stott, P. Anthropogenic impact on Earth's hydrological cycle. *Nat. Clim. Change* **3**, 807–810 (2013).

[115] Lowery, C. M. *et al.* Early Paleocene paleoceanography and export productivity in the Chicxulub Crater. *Paleoceanogr. Paleoclimatol.* **36**, e2021PA004241 (2021).

[116] Dyez, K. A., Cole, J. E. & Lough, J. M. Rainfall variability increased with warming in northern Queensland, Australia, over the past 280 years. *Commun. Earth Environ.* **5**, 117 (2024).

[117] Land, L. S. Diagenesis of skeletal carbonates. *J. Sediment. Res.* **37**, 914–930 (1967).

[118] de Winter, N. J. *et al.* An assessment of latest Cretaceous *Pycnodonte vesicularis* (Lamarck, 1806) shells as records for palaeoseasonality: A multi-proxy investigation. *Clim. Past* **14**, 725–749 (2018).

[119] Morrison, J. O. & Brand, U. An evaluation of diagenesis and chemostratigraphy of upper cretaceous molluscs from the Canadian Interior Seaway. *Chem. Geol. Isot. Geosci. Sect.* **72**, 235–248 (1988).

[120] Zhang, J. Z. & Petersen, S. V. Clumped and oxygen isotope sclerochronology methods tested in the bivalve *Lucina pensylvanica*. *Chem. Geol.* **620**, 121346 (2023).

[121] Hoffman, J. J., Petersen, S. V. & Jones, M. M. Traditional and clumped isotope oyster sclerochronology: Implications for sub-annual temperature and water chemistry variation in the western interior seaway during the mid-cretaceous thermal maximum. *Palaeogeogr. Palaeoclimatol. Palaeoecol.* **658**, 112778 (2025).

[122] Quizon, A. A., Petersen, S. V., de Winter, N. J. & Vellekoop, J. Clumped isotope thermometry (Δ47) measurements in marine gastropods suggest equilibrium precipitation. *Geochim. Cosmochim. Acta* **410**, 234–249 (2025).

[123] Swart, P. K. *et al.* A calibration equation between Δ48 values of carbonate and temperature. *Rapid Commun. Mass Spectrom.* **35**, e9147 (2021).

Supplementary Files

This is a list of supplementary files associated with this preprint. Click to download.

- GCPSupplementaryTextSubmitted.docx
- GCPSupplementalDataSubmitted.xlsx